Available online at www.sciencedirect.com
SCIENCE DIRECT
Journal of Power Sources 157 (2006) 630–640
JOURNAL OF POWER SOURCES
www.elsevier.com/locate/jpowsour

Multi-level reduced-order thermal modeling of electrochemical capacitors

Ph. Guillemet*, Y. Scudeller, Th. Brousse

Laboratoire de Génie des Matériaux, Ecole Polytechnique de l'Université de Nantes, La Chantrerie, rue Christian Pauc, BP 50609, 44306 Nantes Cedex 3, France

Received 7 February 2005; received in revised form 14 July 2005; accepted 20 July 2005
Available online 17 October 2005

Abstract

Ultra capacitors are major components used as power sources offering a combination of high power and high energy. Thermal management of ultra capacitors is one of the main issues for the design of safe powerful systems. This paper presents multi-level electrothermal modeling that can be used to design ultra capacitor structures meeting reliability requirements of power applications. The multi-level modeling is based on both numerical and analytical approaches enabling us to take into account different scales through finite element method computations, shell network models, homogenization methods and ultra-reduced-order model. Basic understanding of electrothermal behavior is performed. Influence of cell characteristics and cooling conditions are studied.

Keywords: Ultra capacitors; Thermal modeling; Thermal resistance; Temperature; Heat sources

1. Introduction

Electrochemical capacitors, so-called supercapacitors or ultra capacitors, are reversible energy storage devices intermediate between secondary batteries and conventional capacitors (Conway [1]). Basically, they offer instantaneous power density more significant than that of batteries and energy density larger than that of dielectric capacitors. Additionally, they can be charged/discharged more than 10^5 times without significant energy loss. Ultra capacitors are attractive for a wide variety of power applications such as telecommunication satellites or hybrid electrical vehicles. In these systems, pulsed power conversion and long-term charge–discharge cycling are required in combination with standard secondary batteries.

Three main classes of materials are used to prepare the electrodes of electrochemical capacitors: carbon (Becker [2]), electronically conducting polymers (Gottesfeld et al. [3]) and metal oxides such as RuO_2 (Trasatti and Buzzanca [4]) or more recently MnO_2 (Lee and Goodenough [5]). These electrode materials are used in aqueous based electrolytes (H_2SO_4, K_2SO_4, etc.) or non-aqueous electrolytes that are characterized by a wider electrochemical stability window relative to aqueous electrolytes. Thus, the combination of a solvent such as acetonitrile or propylene carbonate with different salts (e.g. tetraethylammonium tetrafluoroborate) enabled the increase of the maximum cell potential up to 3 V (Conway [1]). However, despite the remarkable performance of these organic-based systems, they suffer from the use of highly toxic and/or flammable solvents which can cause severe safety hazards. Subsequently, thermal management of the supercapacitors is the main issue for the design of safe powerful systems. This management is actually barely conducted by commercial software that do not take into account the internal layer structure of ultra capacitors.

Pulse power has durations ranging from about 10^{-3} s to 100 s. The move to higher power will continue in the future, and it is now desirable to develop a fundamental understanding of electrothermal behavior of ultra capacitors.

The general aim of this study is to develop multi-level reduced-order thermal modeling of ultra capacitors, including both material properties, structure of electrochemical cells and packaging. The objective, besides a fundamental description of ultra capacitor thermal behavior, is to bring up a useful tool for the design of ultra capacitors and to assess cooling conditions.

2. Temperature and heat production effects on performance

Power losses are produced by charge–discharge current cycles which cause undesirable hot spots affecting both reliabil-

* Corresponding author. Tel.: +33 2 40 68 21 20; fax: +33 2 40 68 21 99.
E-mail address: philippe.guillemet@univ-nantes.fr (Ph. Guillemet).

0378-7753/$ – see front matter © 2005 Elsevier B.V. All rights reserved.
doi:10.1016/j.jpowsour.2005.07.072

Nomenclature

c	specific heat ($J\,K^{-1}\,kg^{-1}$)
d	distance (m)
e	thickness (m)
h	heat transfer coefficient ($W\,m^{-2}\,K^{-1}$)
K_T	terminal thermal conductance ($W\,K^{-1}\,m^{-2}$)
l	distance (m)
N	number of cells
Q_{tot}	total heat source (W)
Q_v	volume heat generation rate ($W\,m^{-3}$)
R	thermal resistance ($K\,W^{-1}$)
t	time
T	temperature (K)
x, y, z	space variables

Greek letters

α, β	dimensionless coefficients
λ	thermal conductivity ($W\,m^{-1}\,K^{-1}$)
ρ	density ($kg\,m^{-3}$)
Φ	heat flux (W)

Subscripts

amb	ambient
c	collector
e	electrode
e+	positive electrode
e−	negative electrode
es	electrode-separator
i	index
is	insulator
s	surface package
tot	total
w	terminal wire

ity and performance. Besides ageing of supercapacitor elements, overheating also induces electrochemical variations of internal characteristics.

Temperature influences greatly the electrochemical behavior of components, like self-discharge. The leakage resistance being higher than the one of conventional capacitors, thermal degradation may occur. Capacitance and leakage resistance of individual cells have to be very constant during the whole life of the device. A uniform temperature is therefore desirable.

Moreover, ultra capacitors have the disadvantage of rather low voltage (1–3 V), so many single cells have to be connected in series in order to achieve several hundred volt capacitor voltage. Capacitors can be destroyed if exposed to transient over voltages. In a series connected string, some cells may be submitted to an over voltage and thermal damage.

Electrothermal behavior of ultra capacitors can be difficult to predict because a large series of transport phenomena (ionic and electronic transport, heat and mass diffusion) and structure heterogeneities are involved. Ultra capacitors form tri-dimensional non-isotropic structures basically composed of interconnected arrays of electrochemical unit cells stacking up

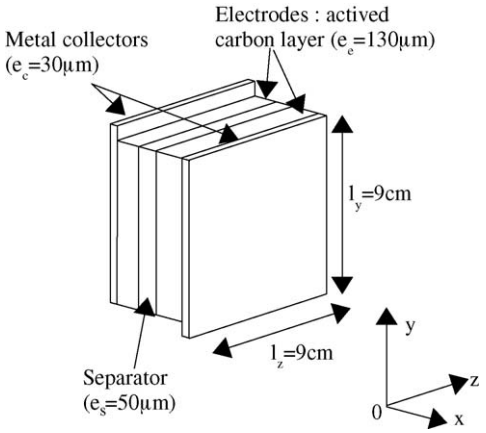

Fig. 1. Investigated unit cell.

to several hundred cylindrical or prismatic unit cells. A wide range of materials is used (composite electrodes, electrolyte and porous separator, metal current collectors, interconnects, package). Temperature profiles depend upon the internally generated power losses that can be non-uniform within electrochemical cells. Current profiles frequency, magnitude of current, unit cell structure, material properties, arrangement of cells, packaging and cooling conditions have a great influence on the working temperature.

3. Description of the electrochemical unit cells

Ultra capacitor bipolar cells consist of high surface area electrode materials loaded with electrolyte (Fig. 1). Negative and positive electrodes are separated by a porous separator impregnated with liquid electrolyte.

Thick film electrodes are composite materials typically prepared by mixing 80% active powder, 7.5% graphite, 7.5% acetylene black and 5% polymer (PTFE).

Symmetric capacitors are assembled from activated carbon powder. Hybrid capacitors are assembled by associating a carbon composite electrode with a MnO_2 electrode in order to increase the cell voltage to values as high as 2.2 V. Due to its potential window of electroactivity, the MnO_2 electrode is used as the positive electrode and carbon as the negative.

For clarity purpose, the design shown in Fig. 1 mentions two activated carbon electrodes. However, models and simulations developed in this study can be applied to any type of cell, such as hybrid aqueous activated carbon/MnO_2 supercapacitor developed by our team (Taberna et al. [7]). Thermal properties of negative and positive electrode depend on their structures, especially the influence of polymer and carbon contents.

Dimensions and properties of the various components are given in Table 1.

4. Finite element analysis

For optimal design purposes, it is desirable to know how the temperature of an electrochemical capacitor varies in space and time in any point of interconnected cells. The relation between

Table 1
Characteristics of carbon–carbon and carbon–MnO_2 supercapacitors, respectively, from [7,8]

	Activated carbon/activated carbon	Activated carbon/MnO_2
Specific capacitance (positive electrode)	95 F g^{-1} (AC)	150 F g^{-1} (MnO_2)
Specific capacitance (negative electrode)	95 F g^{-1} (AC)	105 F g^{-1} (AC)
Electrolyte	$N(et)_4{}^+BF_4{}^-$ in acetonitrile	K_2SO_4 in water
Cell voltage (V)	2.3	2.2
Equivalent serie resistance (Ω cm^2)	≈1	≈2
Power (kW kg^{-1})	44	30
Energy (Wh kg^{-1})	17	15
Charge–discharge test current (A cm^{-2})	≤1	≤1

the heat production rate during repetitive charge–discharge and the temperature $T(M, t)$ at any point of the electrochemical cells is basically ruled by the heat diffusion equation:

$$\nabla \cdot (-\lambda_{(M)} \cdot \nabla \tilde{T}_{(M,t)}) + c\rho \frac{\partial \tilde{T}_{(M,t)}}{\partial t} = \tilde{Q}_{\mathrm{v}} \quad (1)$$

The heat generation rate $\tilde{Q}$ is caused by:

- ionic transport in electrolyte (electrodes and separator) and electronic charge transport in collectors and solid phase of electrodes;
- reversible–irreversible electrochemical reactions at solid–liquid interface of the porous structures;
- thermal contact and electrical resistances between layers.

Electrochemical reactions occur in the positive electrode of the hybrid cells.

During periodic charge–discharge current cycles, the heat generation rate can be decomposed into two components:

$$\tilde{Q}(t) = Q + \delta Q(t) \quad (2)$$

where Q is the mean value reached in steady-state conditions for the periodic repetition rate of the current cycle.

Consequently, the temperature at any point of an electrochemical capacitor can be written as:

$$\tilde{T} = T + \delta T(t) \quad (3)$$

where T is the steady-state temperature. In most charge–discharge repetition rates, dynamic temperature variations can be neglected because the heat diffusion time constant ($\tau \approx 10$ min in the case described in this paper) is largely greater than the electrical pulse period.

The paper investigates the temperature distribution T at any point of electrochemical cells considering Q as a known space function. Q is related to charge transport phenomena (see, for example, Guillemet et al. [8]).

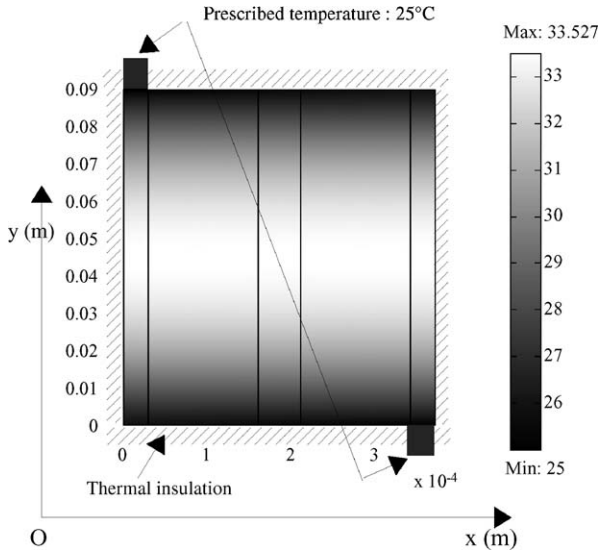

Fig. 2. Temperature distribution in the unit cell, per 1 W per cell heat source.

4.1. Temperature distribution of the electrochemical unit cell

An interconnected bipolar electrochemical cell is considered in this study, in the case where the current flows normal to the current collector from one cell to the next. Temperature is calculated at any point inside the cell using the steady-state heat conduction equation:

$$-\lambda_i \nabla^2 T = Q_i \quad (4)$$

Five different layers are considered: half of the two metal collectors, the negative and positive electrode and the separator. The cell is assumed to be thermally insulated, except the two terminal ends of the collectors (Fig. 2). The temperature of the two terminal ends, the so-called case temperature, is prescribed. Electrical energy is stored in a double layer at the solid–electrolyte interface of the porous electrodes. Heat dissipation is produced into the volume of individual cells, porous electrodes, electrolyte and collectors (see Table 2). The two-dimensional temperature distribution was obtained by the finite element method implemented in Femlab®/Matlab® environment.

Because of the extreme slimness of the cell, the temperature gradient is found to be very weak along the Ox axis (Fig. 2). The huge thermal transfer surface between two adjacent layers favors heat conduction in the Ox direction and allows the Oy gradient to be high. The maximum temperature is located at the medium

Table 2
Thermophysical properties of the electrochemical unit cell

	Thermal conductivity (λ_i) (W m^{-1} K^{-1})	Heat source (W)
Collectors	200	0.05 each
Electrodes	0.5	0.20 each
Separator	0.9	0.50
Total		1

Total dissipated power is 1 W.

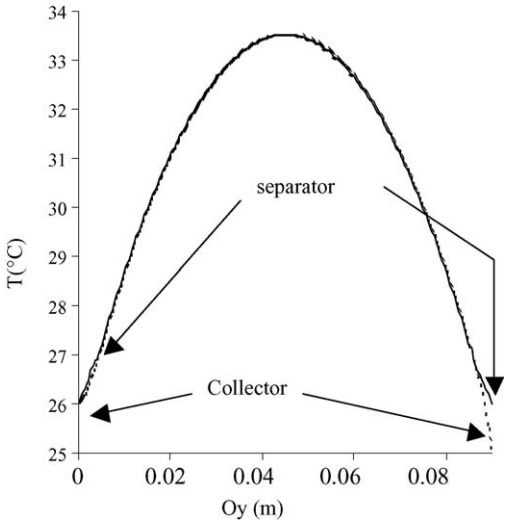

Fig. 3. Temperature inside the cell, along collector and separator, per 1 W per cell heat source.

line of the cell ($y = l_y/2 = 4.5$ cm). The hot spot temperature is quite important (8.5 K W^{-1} above the case temperature) in the conditions of the simulation (Fig. 3). Temperature is roughly the same along each layer of the cell.

4.2. Association of cells

In order to attain high values of capacitance, elementary cells have to be stacked, typically a few hundreds cell associations.

In order to investigate the thermal behavior of such structures, a finite element method (FEM) computation is carried out within an association of 50 cells, with an electrical insulator (thickness: $e_{is} = 400$ μm, thermal conductivity: $\lambda_{is} = 0.4$ W m^{-1} K^{-1}) and an external package (thickness: $e_b = 2$ mm, thermal conductivity: $\lambda_b = 200$ W m^{-1} K^{-1}). The temperature is prescribed at the electrical–thermal interconnects and the external surface ($T_0 = 25$ °C).

The FEM computation in Fig. 4 shows that the temperature distribution of the central cell is not really different from the one investigated in the previous section. However, the cell located at the edge is greatly influenced by the thermal conduction through the package. The high thermal conductivity of the package leads to a quasi-uniform temperature in the near cell, as expected.

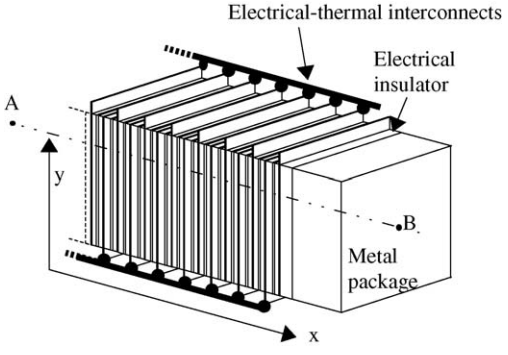

Fig. 4. Temperature distribution in the association of 50 unit cells (FEM computation, per 1 W per cell heat source).

The maximum temperature is reached at the center of the cell association. The hot spot temperature is 8.4 °C over the case temperature, which is very close to the over heating computed in an elementary cell in the previous section.

5. Effect of external cooling conditions

External convection–radiation cooling is commonly considered as the way of avoiding internal overheating of the cells. Such a cooling mode basically consists of air flow at ambient temperature. The cooling rate is then related to the local heat transfer coefficients at the surface package and terminal connections. The heat transfer coefficient on a plane wall in the air at 25 °C, denoted by h_b, is typically between 5 W m^{-2} K^{-1} for natural convection and 200 W m^{-2} K^{-1} for turbulent forced convection.

The effect of thermal–electrical interconnects with the supply wires is often underestimated. In the case of an ultra capacitor, the large contact surface between electrodes and collectors and the high thermal conductivity of the collector makes the collectors a very efficient heat spreader (Fig. 5) only if the electrical–thermal interconnects are especially designed.

5.1. Terminal conductance of electrochemical capacitors

Considering the equivalent thermal circuit of the geometry of Fig. 5, a thermal resistance R_T between end collectors and surrounding air, can be calculated neglecting thermal resistance of metal bounding and thermal contact resistance between bounding and collectors:

$$R_T = R_c + R_w \tag{5}$$

where R_c is the thermal resistance of N collector cells connected in parallel to the metal bounding:

$$R_c = \frac{e_c}{\lambda_c l_c d_c} \times \frac{1}{N} \tag{6}$$

and where R_w is the equivalent thermal resistance of the terminal wire, subjected to air flow, calculated from the basic approximation of extended surfaces [9]. The terminal wire is considered as

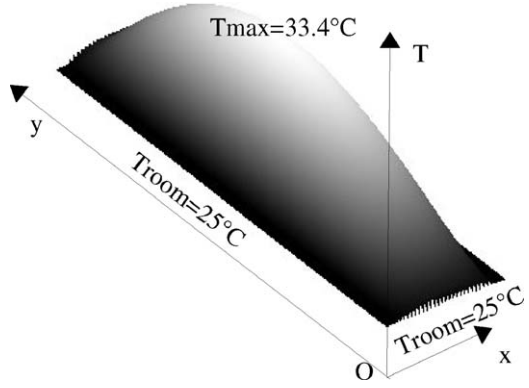

Fig. 5. Thermal drain due to electrical connections (electrical connections on lower side of cells are identical and not drawn).

an infinite fin of uniform cross-sectional area:

$$R_w = \frac{1}{\lambda_w M \left(\pi \frac{d_w^2}{4}\right)} \quad (7)$$

The fin factor M is:

$$M = \sqrt{\frac{4h_w}{\lambda_w d_w}} \quad (8)$$

Using common values: $h_w = 100\,W\,m^{-2}\,K^{-1}$, $\lambda_w = 200\,W\,K^{-1}\,m^{-1}$, $d_w = 5\,cm$, $e_c = 60\,\mu m$, $\lambda_c = 200\,W\,K^{-1}\,m^{-1}$, $l_c = 3\,cm$, $d_c = 1\,cm$, $N = 50$, one obtains: $R_{tot} = 0.96\,K\,W^{-1}$. The equivalent conductance can be considered as a collector boundary conductance (or terminal conductance K_T) in the thermal model, uniformly distributed on the whole upper (or lower) surface of the collectors:

$$K_T = \frac{\frac{1}{R_{tot}}}{N \times (l_y e_c)} \quad (9)$$

The order of magnitude of K_T is thus $3860\,W\,m^{-2}\,K^{-1}$. This is quite a high conductance value, much higher than ones with convection flow on a simple wall. The origin of these phenomena is due to the large exchange surface offered by the terminal wire in air. Therefore, in the case of natural convection cooling, the terminal conductance value can be estimated around few $100\,W\,m^{-2}\,K^{-1}$, and in case of turbulent convection cooling, it might be possible to reach $20{,}000\,W\,m^{-2}\,K^{-1}$.

5.2. Hot spot temperature as a function of external cooling conditions

In the FEM computations above, a prescribed temperature has been applied on the terminal end of collectors as a boundary condition. It means an infinite value of K_T which is not reachable in practical situations. Using different values of terminal conductance and heat transfer coefficient in a third kind of boundary condition on the collectors, different hot spot temperatures are obtained, in Figs. 6 and 7.

Fig. 6 shows that when the electrical connections are thermally improved (highest terminal conductance K_T), the hot spot temperature is lower, as expected, and mainly independent of the external cooling rate (h_b value): most of heat is evacuated through electrical terminal ends.

Fig. 7 shows that for any value of h_b, the hot spot temperature remains strongly dependent on the value of K_T. In those conditions, it is obvious that a poor electrical contact between the terminal wire and the collector ends not only generates an additional heat source, but also adds a thermal resistance that lowest value of K_T.

This asserts that great attention has to be given to thermal design of the electrical connections as well as to their cooling.

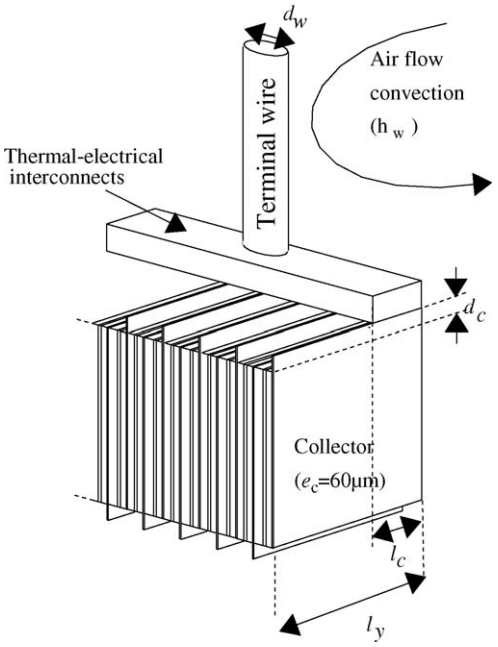

Fig. 6. Maximum temperature in the cell collection vs. boundary cooling of package, for extreme boundary conditions of collector, per 1 W per cell heat source.

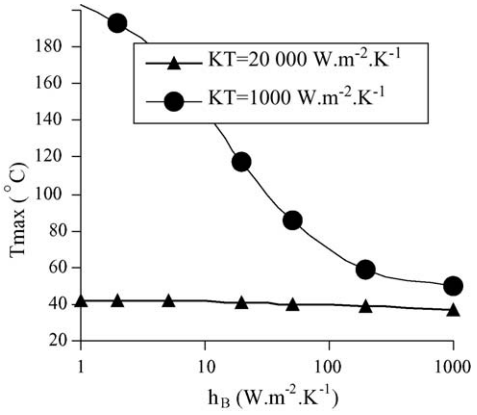

Fig. 7. Maximum temperature in the cell collection vs. boundary cooling of collectors, for extreme boundary conditions of package, per 1 W per cell heat source.

6. Correlation between surface and hot spot temperature

Considering that the temperature dependence of super capacitor parameters (capacitance, resistance, ...) requires that the definition of the "cell temperature" is clear leads to the problem of the temperature measurement. The most easy and most used way to measure the "super capacitor temperature" is to tape a thermocouple or a platinum probe to an electrical connection of the package, close to the collectors. Because the thermal resistance between the center of each cell and the end of the collector is not negligible, the maximum cell temperature is not the one that is measured (see Fig. 8). Moreover, the difference between those two temperatures cannot be considered as constant in so far

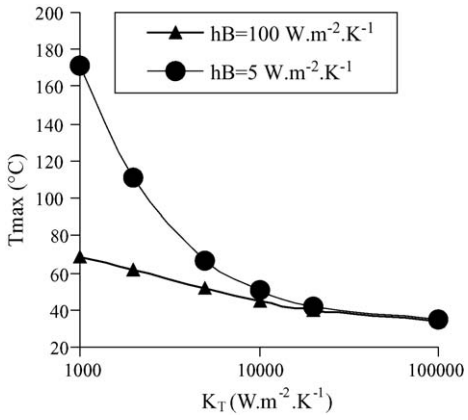

Fig. 8. Error measurement, between hot spot temperature and collector temperature vs. collector heat transfer coefficient, per 1 W per cell heat source.

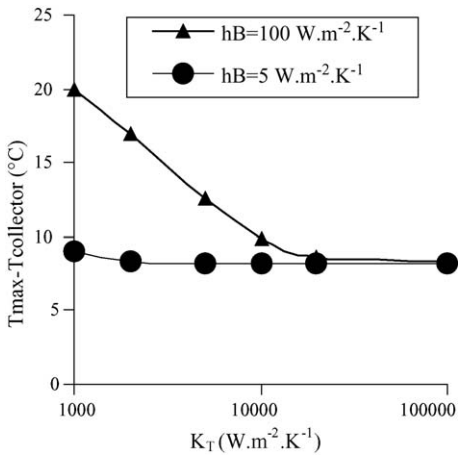

Fig. 9. Description of the association of elementary cells as a shell network.

as it depends widely on the value of the heat transfer coefficient h_B and conductance K_T.

Fig. 8 points out that the error measurement ($T_{max} - T_C$) is weak and independent of the cooling rate of terminal end of the collectors (K_T) when the cooling rate of the package is weak ($h_B = 5\ W\ m^{-1}\ K^{-1}$), but increases roughly and becomes strongly dependent of K_T in the case of an efficient package cooling rate ($h_B = 100\ W\ m^{-1}\ K^{-1}$).

7. Reduced-order thermal modeling

Besides FEM computations, there is a need for a simple but accurate thermal model that could be used in the design of ultra capacitors and for prediction of hot spots.

7.1. Heat sources equivalent distribution

Because of the weak *Ox* temperature gradient, the temperature distribution of the cell can be calculated under the assumption that heat sources are localized inside the collectors. To validate this assumption, a simulation was done, close to the simulation described in Section 3.

The total heat source is kept (1 W per cell), but this power density is no longer distributed in the separator and the electrodes, but concentrated in the collectors (see Table 3). Results show that this approximation leads to an overestimation of only 0.2% of the hot spot temperature rise. The good agreement between the exact distribution of the heat source and localized heat source approximation reduces the problem of identification of microscopic inner heat sources due to volume joule effects, thermal contact resistance, electrochemical reactions, ... A global calorimetric measurement is sufficient, a priori, to characterize all of those heat sources.

Table 3
Power density repartition in the layers of the cell, in case of distributed heat sources or localized heat source approximation

	Distributed sources	Localized sources
Collectors ($W\ m^{-3}$)	2.00×10^5	2.00×10^6
Electrodes ($W\ m^{-3}$)	1.85×10^5	0
Separator ($W\ m^{-3}$)	1.20×10^6	0
Total (W)	1	1
$T_{max} - T_{amb}$ (°C)	8.5	8.5

7.2. Shell network modeling

In this model, the association of N elementary cells is considered, in steady-state conditions, as an array of N collectors where total heat generation rate is concentrated, separated by an equivalent resistive element that models the two electrodes and the separator (Fig. 9). Therefore, the equivalent thermal conductivity of the multi-layered structure electrode–separator–electrode in the *Ox* direction from one collector to the next is introduced. The equivalent thermal circuit leads to the following relation:

$$\lambda_{es}^{-1} = 2\beta \cdot \lambda_e^{-1} + (1 - 2\beta) \cdot \lambda_s^{-1} \tag{10}$$

with $\beta = \frac{\ell_e}{\ell_e + \ell_s}$. All of the elements are considered as a homogeneous medium. The boundary conditions are: prescribed temperature on one of the two extremities of each collector (or infinite value of h_c) and on metal package side walls, thermal insulation elsewhere. These boundary conditions are the best to test the validity of the thermal models because they involve the highest temperature gradients in the medium.

An energy balance, based on the extended surface approximation, so-called shell approximation [9], leads to, for the first element (surface package):

$$\frac{d^2 T_1(y)}{dy^2} - (\gamma_b + \gamma_0) T_1(y) + \gamma_0 T_2(y) = -\gamma_b T_{amb} \tag{11}$$

with $\gamma_b = \frac{h_b}{\lambda_b l_b}$ and $\gamma_0 = \frac{\lambda_{is}}{\lambda_b l_b l_{is}}$. Then, for the following elements (N collectors), from $i = 1$ to N:

$$\frac{d^2 T_i(y)}{dy^2} + \gamma T_{i-1}(y) - 2\gamma T_i(y) + \gamma T_{i+1}(y) = -\frac{Q}{\lambda_c} \tag{12}$$

with $\gamma = \frac{\lambda_{es}}{\lambda_c l_{es} l_c}$, and for the last element (surface package):

$$\frac{d^2 T_{N+1}(y)}{dy^2} + \gamma_0 T_N(y) - (\gamma_b + \gamma_0) T_{N+1}(y) = -\gamma_b T_{amb} \tag{13}$$

The simultaneous equations (Eqs. (11)–(13)) can be written as:

$$\frac{d^2[T(y)]}{dy^2} - [G][T(y)] = [Q] \tag{14}$$

where $[T]$ is the temperature vector $T_i(y)$. The solving method uses eigenvalue matrix computation. In the eigenvectors space, Eq. (14) becomes:

$$\frac{d^2[\theta_0(y)]}{dy^2} - [G_0][\theta_0(y)] = [Q_0] \tag{15}$$

where $[G_0]$ is the eigenvalues diagonal matrix, η_j, of the matrix $[G]$ and $[P]$ is the transformation matrix, as:

$$[G_0] = [P]^{-1}[G][P] \tag{16}$$

The matrix $[\theta_0(z)]$ and $[Q_0]$ are:

$$[Q_0] = [P]^{-1}[Q] \quad \text{and} \quad [\theta_0(z)] = [P]^{-1}[T(y)]$$

The general solution of Eq. (15) is, from $i=0$ to $(N+1)$:

$$\theta_{0i}(y) = \Omega_i ch((y-L)m_i) + \Lambda_i sh((y-L)m_i) - \frac{Q_{0i}}{m_i^2} \tag{17}$$

where

$$m_i = \sqrt{\eta_i} \tag{18}$$

The constant factors Ω_i and Λ_i are determined from boundary conditions:

$$T(0) = T_{amb} \quad \text{and} \quad \left.\frac{dT(y)}{dy}\right|_{y=L} = 0 \tag{19}$$

for even values of i, and:

$$T(L) = T_{amb} \quad \text{and} \quad \left.\frac{dT(y)}{dy}\right|_{y=0} = 0 \tag{20}$$

for odd values of i.

The temperature can be calculated, then, in each collector, along the Oy axis. Results show a good agreement with the FEM computation, except a moderate underestimation of the hot spot temperature ($T_{max} - T_{amb} = 8.2\,^{\circ}C$ for shell network model, $8.4\,^{\circ}C$ for FEM computation).

7.3. Homogenization method

It is of interest to apply the standard homogenization method in the case of the ultra capacitor layout. This method is commonly used for the thermal modeling of various electrochemical storage systems (see, for example, refs. [10,11]).

The multi-layered structure of the capacitor is replaced by homogeneous orthotropic structure having equivalent thermal properties and where the heat source is uniformly spread throughout the whole volume. The thermal conductivity in the direction normal to the collectors (x axis) is then:

$$\lambda_x^{-1} = \alpha \cdot \lambda_c^{-1} + (1-\alpha) \cdot \lambda_{es}^{-1} \tag{21}$$

with $\alpha = \frac{\ell_c}{\ell_c + \ell_{es}}$ and where λ_{es} is defined as in the previous section.

Table 4
Recap of the different "hot spot to case" thermal resistances obtained by the different models

	Thermal resistance ($K\,W^{-1}$)
Finite element method	8.4
Localized sources	8.4
Shell network model	8.2
Homogenization method	8.2
Ultra-reduced-order model	7.2

The thermal power is considered to be 1 W per cell and can reach few Watts per cell in practical situations.

The thermal conductivity in the transverse direction (y axis) is then:

$$\lambda_y = \alpha \cdot \lambda_c + (1-\alpha) \cdot \lambda_{es} \tag{22}$$

Using the values given in Section 3 (see Table 4), one obtains: $\lambda_x = 0.64\,W\,m^{-1}\,K^{-1}$ and $\lambda_y = 32.9\,W\,m^{-1}\,K^{-1}$.

An FEM computation of the heat conduction equation in the cell with equivalent Ox and Oy direction thermal conductivities, thermal insulation on side boundaries and prescribed temperature on upper and lower boundaries (Fig. 10) leads to the temperature field shown in Fig. 11.

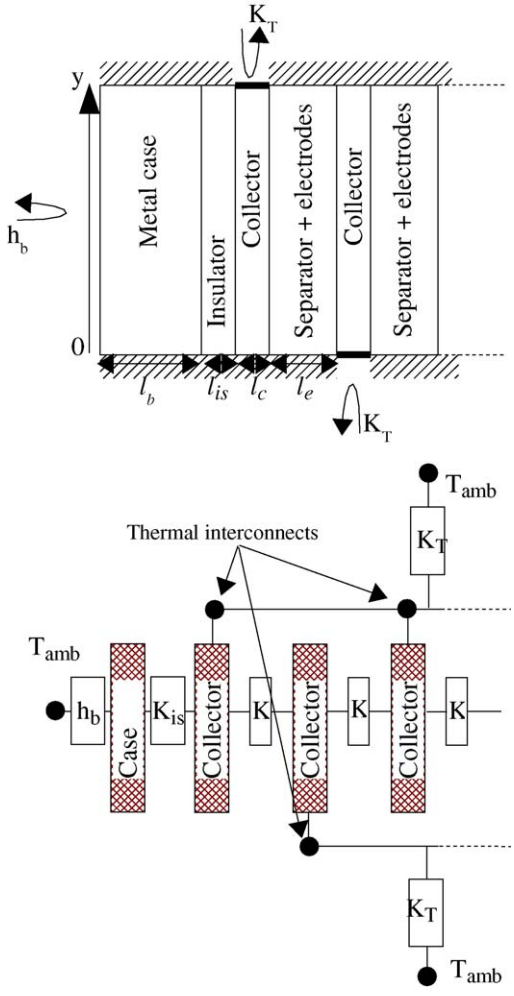

Fig. 10. Conductivities and geometry of an elementary cell (top) and equivalent homogeneous element (bottom).

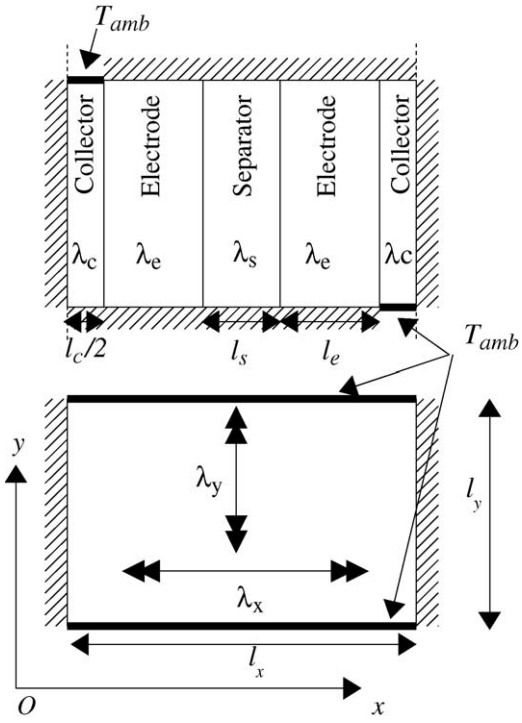

Fig. 11. Temperature field in the elementary cell, at $x = l_x/2$, comparison between the exact heterogeneous model and the homogeneous approximation.

The maximum temperature elevation is found to be 10.0 °C in the homogeneous approximation, instead of 10.6 °C in the exact heterogeneous model, applied to a unique cell (Section 3).

In the case of the association described in Fig. 12, the calculation is nearly the same. The thermal conductivities of the whole homogeneous medium are the same as for a single cell ($\lambda_x = 0.643\ \mathrm{W\,m^{-1}\,K^{-1}}$ and $\lambda_y = 32.9\ \mathrm{W\,m^{-1}\,K^{-1}}$) but the insulator and package layers have to be taken into account through thermal resistances. The surface conductance is then:

$$K_y = \frac{1}{\frac{l_B}{\lambda_B} + \frac{l_{is}}{\lambda_{is}}} \tag{23}$$

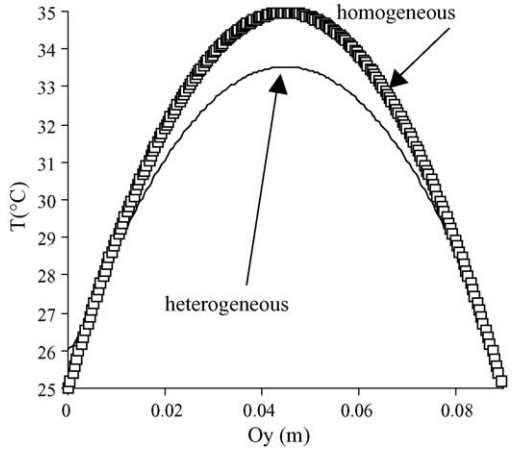

Fig. 12. A few cells from the association of 50 elementary cells.

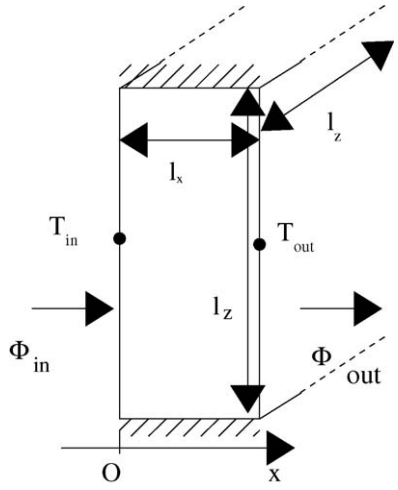

Fig. 13. 1D heat transfer in an homogeneous slab.

Using the values given in Section 4.2, the hot spot temperature is now 8.2 °C over ambient temperature, instead of 8.4 °C obtained by FEM computation on a heterogeneous model, applied to the association of Section 4.2. This result is quite good: the homogenization method is fully applicable to the case of ultra capacitors.

7.4. Ultra-reduced-order modeling

7.4.1. Four port matrix formalism for 1D heat conduction analysis

Four port matrix formalism can be used for 1D heat conduction analysis with internal heat production.

Consider the 1D heat conduction in a slab of homogeneous medium of Fig. 13. Solution of the heat conduction equation leads to Eqs. (A.8) and (A.11), giving relations between temperature and heat flux at terminal ends and heat generation rate:

$$T_{out} = -Q_{tot}\frac{R}{2} - R\Phi_{in} + T_{in}$$

$$\Phi_{out} = Q_{tot} + \Phi_{in}$$

Eqs. (A.8) and (A.11) can be transformed in a matrix relation, between in and out values:

$$\begin{pmatrix} T_{out} \\ \Phi_{out} \end{pmatrix} = \begin{pmatrix} 1 & -R \\ 0 & 1 \end{pmatrix} \begin{pmatrix} T_{in} \\ \Phi_{in} \end{pmatrix} + \begin{pmatrix} Q_{tot}\frac{R}{2} \\ Q_{tot} \end{pmatrix} \tag{24}$$

This relation describes the thermal behavior of the slab.

7.4.2. Equivalent thermal circuit

Consider the thermal circuit of Fig. 14. The energy balance is obviously:

$$\Phi_{out} = Q_{tot} + \Phi_{in} \tag{25}$$

which is no more than Eq. (A.11). The incoming flux is:

$$\Phi_{in} = \frac{T_{in} - T_0}{\frac{R}{2}} \tag{26}$$

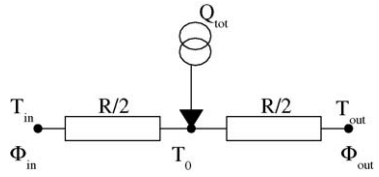

Fig. 14. Equivalent thermal circuit from the homogeneous slab of Fig. 13.

A heat flux balance, at the node O, leads to:

$$\frac{T_{\text{in}} - T_0}{\frac{R}{2}} + Q_{\text{tot}} + \frac{T_{\text{out}} - T_0}{\frac{R}{2}} = 0 \tag{27}$$

Eliminating T_0 between those two relations leads exactly to Eq. (A.8): the circuit of Fig. 14 is the equivalent thermal circuit of the slab in Fig. 13, i.e. to the matrix equation (Eq. (24)), in term of input–output quantities. It enables the calculation of in- and out-temperature and fluxes (T_{in}, T_{out}, Φ_{in}, Φ_{out}) but not of the temperature inside the medium: the temperature T_0 at the central node of Fig. 14 is not a physical temperature but a mathematical one, on a virtual point. Once the input and output quantities have been determined, the hot spot temperature has to be calculated using the heat conduction equation in the medium, which can be very easy as shown below.

7.4.3. Application to an ultra capacitor

The reduced-order model, detailed in the above section, is convenient and easy to use. It enables one to get quickly a rough approximation of the hot spot temperature in an ultra capacitor.

The equivalent thermal circuit of the association described in Fig. 4 is shown in Fig. 15. It takes into account the heat flow in both Ox and Oy directions. Four additional thermal resistances have been included in the equivalent circuit. They represent the boundary conditions:

$$-\lambda \left.\frac{\mathrm{d}T}{\mathrm{d}x}\right|_{x=0} = \frac{\Phi_{x_{\text{in}}}}{l_y l_z} = h_{\text{B}}(T_{x0} - T_{\text{air}}) \tag{28}$$

$$-\lambda \left.\frac{\mathrm{d}T}{\mathrm{d}x}\right|_{x=l_x} = \frac{\Phi_{x_{\text{out}}}}{l_y l_z} = h_{\text{B}}(T_{x0} - T_{\text{air}}) \tag{29}$$

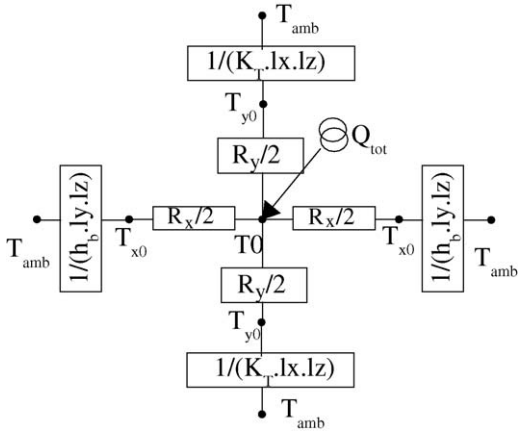

Fig. 15. Equivalent thermal circuit from the ultra capacitor of Fig. 4.

$$-\lambda \left.\frac{\mathrm{d}T}{\mathrm{d}y}\right|_{y=0} = \frac{\Phi_{y_{\text{in}}}}{l_x l_z} = K_T(T_{y0} - T_{\text{air}}) \tag{30}$$

$$-\lambda \left.\frac{\mathrm{d}T}{\mathrm{d}y}\right|_{y=l_y} = \frac{\Phi_{y_{\text{out}}}}{l_x l_z} = K_T(T_{y0} - T_{\text{air}}) \tag{31}$$

In this diagram, R_i is the thermal resistance in the Ox or Oy direction:

$$R_x = \frac{N l_x}{\lambda_x l_y l_z} \tag{32}$$

$$R_y = \frac{l_y}{\lambda_y l_x l_z} \tag{33}$$

The thermal conductivities λ_x and λ_y have been calculated in Eqs. (21) and (22).

Eq. (36) is the same as Eq. (23), it takes into account the thermal resistance of the insulator and package walls. Calculation of T_0 is now obvious, using the energy balance at the node O, for example:

$$Q_{\text{tot}} - 2\left(\frac{T_0 - T_{\text{amb}}}{\frac{R_x}{2} + \frac{1}{h_{\text{B}} l_y l_z}}\right) - 2\left(\frac{T_0 - T_{\text{amb}}}{\frac{R_y}{2} + \frac{1}{K_T l_x l_z}}\right) = 0 \tag{34}$$

According to the previous boundary conditions (prescribed temperature on upper and lower sides and on external package walls), the two surface conductances become:

$$K_T = \infty \tag{35}$$

$$h_{\text{B}} = \frac{1}{\frac{l_{\text{B}}}{\lambda_{\text{B}}} + \frac{l_{\text{is}}}{\lambda_{\text{is}}}} \tag{36}$$

Solving this equation leads to the value of T_0 which has no physical meaning but it enables one to calculate T_{x0} and T_{y0} (see Fig. 15):

$$\begin{aligned} T_{\text{amb}} - T_{x0} &= \frac{T_{\text{amb}} - T_0}{\frac{R_x}{2} + \frac{1}{h_{\text{B}} l_y l_z}}\left(\frac{1}{h_{\text{B}} l_y l_z}\right) \\ T_{\text{amb}} - T_{y0} &= \frac{T_{\text{amb}} - T_0}{\frac{R_y}{2} + \frac{1}{K_T l_x l_z}}\left(\frac{1}{h_{\text{C}} l_x l_z}\right) \end{aligned} \tag{37}$$

Using again the values given in Section 4.2, the temperatures are: $T_{x0} = 25.9\,^{\circ}\text{C}$ and $T_{y0} = 25.0\,^{\circ}\text{C}$ (prescribed temperature).

To complete the calculation, the hot spot temperature, in the middle of the cell association, can be evaluated with a basic approximation. The application of Eq. (A.4), in the 1D heat transfer it describes, with $x = l_x/2$ leads to $Q_{\text{tot}} - 4\frac{T_{x=l/2} - T_{\text{in}}}{\frac{R}{2}} = 0$. In the 2D heat transfer of Fig. 15, this expression can be extended as:

$$Q_{\text{tot}} - 4\left(\frac{T_{\max} - T_{x0}}{\frac{R_x}{2}}\right) - 4\left(\frac{T_{\max} - T_{y0}}{\frac{R_y}{2}}\right) = 0 \tag{38}$$

where T_{max} is the hot spot temperature. Using again the values given in Section 4.2, one obtains: $T_{max} - T_{amb} = 7.2\,^{\circ}C$. The discrepancy between this result and the FEM result (8.4 °C) is about 16% which is not too much, considering the ease of this method to calculate the hot spot temperature using only three basic equations (Eqs. (34), (37) and (38)).

8. Summary of models and results

The numerical FEM computation of Section 4.2 and the four semi-analytical models developed in Section 7 have both been conducted in the same configuration of $N = 50$ associated cells (Fig. 12), with a heat source of 1 W per cell and with a prescribed connection temperature, involving the most important temperature gradients in the Oy and Ox directions and leading to the determination of the "hot spot to case" resistance.

The finite element method gives the most accurate results of the temperature distribution anywhere in the medium, but it is a weighty numerical method.

The shell network model enables the analytical computation of the temperature distribution in the collectors and leads to a 15% underestimation of the hot spot temperature rise with respect to ambient temperature.

The homogenization method gives very good results (less than 2% underestimation in the studied case). Although it is a numerical method, this approximation leads to a large decrease of computing time compared to the FEM method, considered as reference in a lack of experimental measurements.

The ultra-reduced-order model offers the great advantage of providing an easy and fast analytical calculation of the hot spot temperature in an ultra capacitor: this model is to be used in most practical case where a high accuracy is not needed. For example, thermal security predictions always include a large safety range which is usually wider than the accuracy of the model.

9. Application to a parametric study

The reduced-order model leads to a rapid and accurate estimation of the hot spot cell temperature, depending on a wide range of parameters: the cooling rate, the properties and size of constituting materials, the dissipated power source as function of repetition rate of current cycles.

It is of interest, for example, to evaluate the influence of collector conductivity on this temperature. Eqs. (21) and (22) give the dependence of the conductivity values of the homogeneous equivalent medium λ_x and λ_y, then Eqs. (32) and (33) give the resistance values R_x and R_y and finally Eq. (38) gives the hot spot overheating for a 1 W heat source, which is the thermal resistance of the ultra capacitor.

Fig. 16 shows that decreasing the collector conductivity from $400\,W\,m^{-1}\,K^{-1}$ down to $40\,W\,m^{-1}\,K^{-1}$ increases the thermal resistance from $4\,K\,W^{-1}$ up to $22\,K\,W^{-1}$.

Moreover, the comparison between this basic model (so-called ultra-reduced-order model) based on multi-port element network and the exact FEM computation (Fig. 16) shows the validity of the approximation over a wide range of materials and sizes.

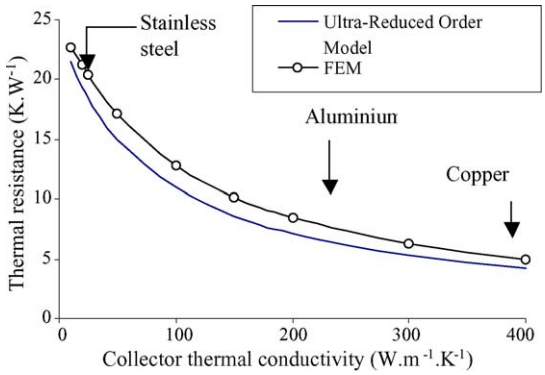

Fig. 16. Influence of collector thermal conductivity on the "hot spot to case" thermal resistance.

10. Application to thermal safety

The thermal resistances given in the previous section were obtained with $Q = 1$ W per cell (81 cm^2). In practice, the thermal power can be much more than 1 W, especially in high intensity current applications that are the main application field of ultra capacitors. Consider the case of an ultra capacitor with $5\,\Omega\,cm^{-2}$ ESR and $0.33\,F\,cm^{-2}$ capacitance. A 200 mA current intensity (equivalent to 166 A in a 2500 F association) leads to 1.8 W per unit cell and consequently to about 15 K overheating. This overheating can be detrimental in high ambient temperature ($T_{amb} = 40\,^{\circ}C$) and low cooling rate ($T_{case} = 60\,^{\circ}C$). In those conditions, the hot spot temperature reaches 75 °C and can overtake the safety limit of running temperature (70 °C for acetonitrile solvent) and cause serious damage.

11. Future works

The present work is a preliminary study to future works that intend to achieve a complete description of heat transport phenomena in ultra capacitors, including other geometries, other materials, thermal transient analysis as well as thermal measurement (temperature change, dissipated power, thermophysical properties of constituting layers).

12. Conclusion

Thermal analysis of super capacitors points out that the maximum temperature is reached at the center of the cell association, as expected. This maximum temperature is, to a large extent, different from the collector temperature that can be measured outside the package. Moreover, this hot spot temperature cannot be easily related to the outside temperature because it depends widely on the way the heat is thrown away from the cell association.

In order to evacuate heat produced from cells, special attention must be given to the cooling performance of the electrical connections of the collectors, where the most important part of temperature rise is located.

Temperature inside the ultra capacitor, or thermal resistance, can be calculated using four models, corresponding to four levels of thermal analysis:

- Finite element method gives the most accurate temperature and flux values, but is a weighty method.
- The shell network model leads to a semi-analytical calculation of the temperature in each layer of the capacitor under the assumption that heat transfer is longitudinal from one to the next collector and in the axial direction through the collectors.
- The homogenization technique gives a good estimation of the temperature everywhere in the capacitor, assuming that the cell association is a homogeneous non-isotropic structure.
- The ultra-reduced-order model, based on the thermal properties homogenization and an equivalent thermal circuit leads to a simple but rather good estimation of the thermal resistance of the capacitor and enables easy study of any parameter influence on this thermal resistance. This model is to be used in most practical situation where a high accuracy is not needed, like thermal security prediction, for example.

Acknowledgment

This work is supported by MENRT/DGA/CNRS (CAPRYS project PR6-2, ACI Energie 2003).

Appendix A

The 1D heat conduction equation, in the slab, is, per volume unit:

$$-\lambda\frac{\mathrm{d}^2T}{\mathrm{d}x^2} = Q \tag{A.1}$$

where Q is the volumetric heat source ($\mathrm{W\,m^{-3}}$). In a general case, among the four boundary equations:

$$T(x=0) = T_{\mathrm{in}}, \qquad -\lambda\left.\frac{\mathrm{d}T}{\mathrm{d}x}\right|_{x=0} = \frac{\Phi_{\mathrm{in}}}{l_y l_z} \tag{A.2}$$

$$T(x=l_x) = T_{\mathrm{out}}, \qquad -\lambda\left.\frac{\mathrm{d}T}{\mathrm{d}x}\right|_{x=l_x} = \frac{\Phi_{\mathrm{out}}}{l_y l_z} \tag{A.3}$$

two equations constitute the boundary conditions, used to solve this 1D problem.

The general form of the solution of Eq. (A.1) is:

$$T(x) = -\frac{Q}{2\lambda}x^2 + Ax + B \tag{A.4}$$

The integration constants, A and B, can be expressed from Eq. (A.2):

$$B = T_{\mathrm{in}}, \qquad A = -\frac{\Phi_{\mathrm{in}}}{\lambda l_y l_z} \tag{A.5}$$

leading to the expression of $T(x)$:

$$T(x) = -\frac{Q}{2\lambda}x^2 - \frac{\Phi_{\mathrm{in}}}{\lambda l_y l_z}x + T_{\mathrm{in}} \tag{A.6}$$

and to the heat flux:

$$-\lambda\frac{\mathrm{d}T}{\mathrm{d}x} = Qx + \frac{\Phi_{\mathrm{in}}}{l_y l_z} \tag{A.7}$$

Applying Eq. (A.6) with $x = l_x$, one obtains:

$$T_{\mathrm{out}} = -Q_{\mathrm{tot}}\frac{R}{2} - R\Phi_{\mathrm{in}} + T_{\mathrm{in}} \tag{A.8}$$

where R is a thermal resistance:

$$R = \frac{l_x}{\lambda l_y l_z} \tag{A.9}$$

and Q_{tot} is the total heat power (W) in the slab:

$$Q_{\mathrm{tot}} = Q l_x l_y l_z \tag{A.10}$$

Applying Eq. (A.7) with $x = l_x$, one obtains:

$$\Phi_{\mathrm{out}} = Q_{\mathrm{tot}} + \Phi_{\mathrm{in}} \tag{A.11}$$

which is no more than the energy balance into the slab.

References

[1] B.E. Conway, Electrochemical Supercapacitors, Scientific Fundamentals and Technological Applications, Kluwer Academic Plenum Press, New York, 1999.
[2] H.E. Becker, U.S. Patent 2,800,616 (1957).
[3] S. Gottesfeld, A. Redondo, S.W. Feldberg, J. Electrochem. Soc. 134 (1987) 271.
[4] S. Trasatti, G. Buzzanca, J. Electroanal. Chem. Appl. 29 (1971) 1.
[5] H.Y. Lee, J.B. Goodenough, J. Solid State Chem. 148 (1999) 220.
[7] P.L. Taberna, P. Simon, J.F. Fauvarque, J. Electrochem. Soc. 150 (2003) A292–A300.
[8] Ph. Guillemet, Y. Scudeller, T. Brousse, Electro-thermal analysis of hybrid electrochemical supercapacitors, in: 1st European Symposium on Super Capacitors and Applications, Belfort, 2004.
[9] F.P. Incropera, D.P. DeWitt, Fundamentals of Heat and Mass Transfer, fourth ed., John Wiley & Sons, New York, 1996.
[10] S. Al Hallaj, H. Maleki, J.S. Hong, J.R. Selman, J. Power Sources 83 (1999) 1–8.
[11] C.Y. Wang, V. Srinivasan, J. Power Sources 110 (2002) 364–376.